

## **5.0 MODELLING OF DEFORMATION BEHAVIOR OF LOW ALLOY STEEL**

### **5.1 Introduction**

Generally, the study of ferrous metals is complicated by two crystallographic and magnetic phase changes. Each allotropic change results in a change of properties of the material. The properties depend on the thermo-mechanical treatment and become important for creep resistant low alloy ferritic steels. These alloys derive most of their strength from precipitate hardening; small changes in thermo-mechanical behaviour has large effects on mechanical behaviour.

In low alloy steels the major mechanism responsible for microstructure degradation is coarsening of the carbide precipitates. The mechanism of solute hardening presents some problems. An extension of the precipitation hardening model to individual solute atoms may, at best, apply to very dilute solutions when only interstitial solutes cause any appreciable strengthening. Randomly dispersed substitution solute atoms do not act as discrete obstacles when they are in concentrated solution, but interact with dislocations cooperatively.

The mechanism of forest dislocation cutting exhibits the usual complexities. Forest dislocations can interact with glide dislocation to form attractive junctions where small nodal segments of dislocations can form to significantly lower the local energy of the two intersecting dislocations, making a thermally assisted intersection possible. In work hardened crystals not only are the points of intersection of forest dislocations with slip plane nearly always clustered into cell walls giving a distinctly non random distribution, but they can also be displaced significantly by the forces exerted by impinging glide dislocations as a collection of fixed and randomly distributed point obstacles.

Much attention has been paid to the high temperature creep and fracture behavior of low alloy steels<sup>78,81</sup>. Considerable variations in creep responses have been noted and this has led to several different creep mechanisms being proposed to explain this behavior. These variations are due to the widely differing microstructure which can be produced in the alloy. The creep properties of low alloy ferritic steels are very dependent on heat treatment. Baird et al<sup>78</sup> studied the behavior of 1 pct Mo and 2 ¼ pct Cr-1pct Mo ferritic steels in various micro structural forms and found that creep was recovery controlled only under certain conditions of composition, initial structure and testing conditions. Thus recovery control was related to the presence of Mo<sub>2</sub>C and Mo<sub>2</sub>N particles in the matrix, whilst a solid solution mechanism was suggested as being important for non-recovery controlled creep.

To date there have been several suggestions for the rationalization of creep data<sup>100</sup>. These proposals have often evolved from empirical equations for the stress dependence of the secondary steady state creep rate of the form:-

$$\dot{\epsilon}_s = A\sigma^n \text{Exp}\left(-\frac{Q_c}{RT}\right) \quad 5.1$$

where in pure metals and single alloys  $n$  is often found to be in the range of 4-5,  $Q_c$  it is close to the activation energy for self diffusion.  $A$  is a structure sensitive parameter;  $R$  is the gas constant, and  $T$  the creep temperature.

The creep behavior of complex engineering alloys such as  $\gamma'$  hardened super alloys and other particle strengthened materials, deviates from this general pattern in two main respects. First, a well established steady state creep regime is rarely observed; rather, after a small primary creep regime, the creep rate progressively increases from a minimum value until fracture occurs. Typical creep curves for low alloy ferritic steels illustrate dominance of tertiary creep. When minimum creep

rates are analyzed in terms of equation (5.1), unrealistically high values of  $n$  and  $Q$  are obtained<sup>68</sup>

Several attempts have been made to enhanced creep data correlation. For example, Mclean and Hale<sup>69</sup> demonstrated that the creep rate for pure metals could be brought closer together by dividing stress by the modulus of the material at the appropriate temperature. Because of the equivalent between the activation energy of diffusion and that of self diffusion, Sherby<sup>103</sup> extended the approach by dividing the creep rate by the diffusion coefficient,  $D$ . In addition, it was shown that an improved correlation could result if the stacking fault energy of the metal was also taken into account. The resultant expression<sup>101</sup> had the form.<sup>65</sup>

$$\frac{\dot{\epsilon}_s}{D} = A' \gamma_s^{3-5} \left( \frac{\sigma}{G} \right)^n \quad 5.2$$

with  $A$  a constant and  $G$  the shear modulus. More recently Mukherjee, Bird and Dorn<sup>102</sup> have criticized this equation not only on the ground that it is dimensionally unbalanced but also because they consider that the activation energy term should be stress dependent. Instead they proposed the equation:

$$\frac{\dot{\epsilon}_s K T}{D G b} = A'' \left( \frac{\sigma}{G} \right)^n \quad 5.3$$

where  $A$  is probably a function of  $\gamma_s$ ,  $K$  is the Boltzmann constant, and  $b$  is the burgers vector. When equation (5.3) was used on data for pure metals the scatter band in terms of the maximum to minimum ratio of  $\frac{\sigma}{G}$  was  $\approx 6$  for constant  $\frac{\dot{\epsilon}_s K T}{D G b}$ <sup>100</sup>. It was suggested that a closer correlation could be achieved if the dependence of  $A''$  on  $\gamma_s$  were known. Unfortunately, reliable  $\gamma_s$  values are available only for a limited number of metals and then rarely at the appropriate creep temperature<sup>100</sup>.

## 5.2 PROPOSED MODEL

In describing plastic deformation behavior, both empirical and semi-empirical relations have been considered. The most popular approaches have been the use of non-linear viscoplastic theories and the power law, which are purely empirical, or the use of the semi-empirical kinetic flow equations. Viscoplastic theories describe deformation behavior in terms of combinations of mechanical components such as springs, dashpots and friction elements from which differential equations describing flow may be derived. In the power law description the relation between applied stress amplitude and plastic strain amplitude is expressed as:

$$\sigma_a = k \varepsilon_p^n \quad 5.4$$

where  $k$  and  $n$  are constants that are determined from experimental data fit. In the case of the semi-empirical kinetic equations flow is considered to be thermally activated, and the relationship between applied stress  $\sigma$ , and strain rate  $\dot{\varepsilon}$  is expressed in the form<sup>2,,87</sup>

$$\dot{\varepsilon} = f(\sigma, s) \exp\left[\frac{-\Delta G(\sigma, s)}{kT}\right] \quad 5.5$$

where  $s$  is a structural parameter of the material,  $k$  is Boltzmann's constant,  $T$  is the absolute temperature, and  $\Delta G$  is the change in free energy, which depends on the mechanism of flow. With  $s$  constant in the exponential term and the pre-exponential term being independent of  $s$ , equation (5.10) has the form used to describe steady state flow where deformation is controlled by dislocation glide through obstacle fields such as forest dislocations or precipitates<sup>2,,87</sup>

Although purely empirical models may describe the observed behavior with some degree of accuracy, they fail to address the internal state variables of the material. For instance, the use of the power law relation of the form of equation (5.4) implies that a log-log plot should give a straight-line relation. However, for some metals, e.g. polycrystalline copper, the

double-log plot is not linear<sup>87</sup>. This is probably due to the inability of the power law empirical relation to account for the internal state variable(s) of the material. Therefore for such materials, and also for materials development purposes, a model that accounts for the internal state variables and their evolution during deformation may give a more accurate description of behavior. Such a model is made possible by means of constitutive equations.

A common approach to establishing a constitutive relation is to find an equation describing the mechanical response at a fixed structure, as specified by a certain state, or by structural parameters. Such equation is referred to as a kinetic equation, and is complemented with evolutionary equations for these structure parameters. In general, the kinetic model may be governed by more than one structural parameter evolving with different rates towards the respective steady state values.

At low temperatures, plasticity (both plastic deformation and creep) is glide-controlled and a suitable kinetic equation that governs the flow behavior is given by<sup>2</sup> :-

$$\dot{\gamma}_p = v_0 \left( \frac{\sigma_s}{\mu} \right)^2 \exp \left\{ - \frac{\Delta F}{kT} \left[ 1 - \left( \frac{\sigma_s}{\tau} \right)^p \right]^q \right\} \quad 5.6$$

where,  $\dot{\gamma}_p$  is the plastic shear strain rate,  $v_0$  is a frequency term,  $\sigma_s$  is applied shear stress,  $\Delta F$  is the activation energy required to overcome obstacles;  $k$  is Boltzmann constant;  $T$  is the absolute temperature;  $\tau$  is the athermal flow strength of the material, (i.e. shear stress in the absence of thermal energy);  $p$  and  $q$  ( $0 \leq p \leq 1$ ,  $1 \leq q \leq 2$ ) are constants, and represent the obstacle shape.

The single- parameter model, although capable of describing the static creep and monotonic loading behavior in a satisfactory manner is limited in scope. The limitation of the one-parameter approach is due to the neglect of other state parameters whose fast relaxation may be

responsible for transient behavior. Due to the possibility of more than one structural parameter governing flow, Estrin and Kubin<sup>10</sup> consider mobile and forest dislocations as two structural parameters that govern flow, but studies were limited to the case of monotonic loading.

Both plastic deformation and creep occur as a result of the applied shear stress exerting forces on defects such as dislocations in the material, causing them to move. Thus, at the same temperature it is expected that both plastic deformation and creep can be controlled by the same mechanisms and differ only in the boundary condition. Therefore, realistically, a model that describes plastic deformation should describe creep as well.

A major objective of this work is to develop mathematical relations that are capable of describing the correlation between tensile and softening responses of the material, in this case low alloy steel. Two types of mechanism were observed. Low temperatures and high stresses were characterized by jerky glide whilst high temperature and low stress were characterized by some form of power creep phenomenon.

This section discusses a unified model that has the potential of describing monotonic work hardening and static creep behavior. The model considers low temperature deformation situations where flow is thermally activated and controlled by the glide motion of dislocations in the presence of microscopic obstacles, and is consistent with the mechanism of dislocation blocking and subsequent re-mobilization (at least partially) on stress reversal.

The overall plastic behaviour of a metal can conveniently be modelled in terms of a pair of coupled differential equations. One of these describes the strain rate in terms of the externally imposed testing conditions, together with an internal structure variable. The other should describe the evolution of the internal structure term and include any hardening or softening processes. Softening processes in low alloy steels are expected

to be due to recovery of dislocation forest structures and/or precipitate growth. Previous work has suggested that the former controls softening during creep<sup>5</sup> and this is assumed to be the dominant effect in the material and over the test conditions studied during this investigation. Thus creep behaviour was modelled in terms of an equation describing plastic deformation together with one describing recovery.

It also considers that the total dislocation density consists of mobile and obstacle (forest) components: the generation and glide motion of mobile dislocations are responsible for plastic flow and occur as a result of the applied shear stress while the build-up of forest dislocations causes hardening through the structure parameter. Conversely, the immobilization and/or loss of mobile dislocations enhance hardening while the breakdown of cell structures promotes softening.

The mobile and forest dislocation densities  $\rho_m$  and  $\rho_f$  are related to the applied shear stress  $\sigma_{sc}$  and obstacle strength  $\tau_t$ , respectively as<sup>2</sup>

$$\sigma_{sc} = \alpha\mu b\rho_m^{1/2} \quad 5.7a$$

$$\tau_t = \alpha\mu b\rho_f^{1/2} \quad 5.7b$$

The subscripts, *c* and *f* attached to the shear stress and athermal strength serve to indicate that equation (5.7), is applicable to both monotonic and cyclic deformation and that the athermal strength is due to the forest dislocation density. The mobile dislocation density and hence the applied shear stress evolve with strain as:-

$$\frac{d\sigma_{sc}}{d\gamma} = 0.5\alpha\mu b\rho_m^{-1/2} \frac{d\rho_m}{d\gamma} \quad 5.8$$

Similarly, the evolution of the  $\tau_t$  with strain is given as:

$$\frac{d\tau_i}{d\gamma} = 0.5c_2\alpha\mu b\rho_f^{-1/2}\frac{d\rho_f}{d\gamma} \quad 5.9$$

In general, the evolution rate of each of these dislocation densities can be expressed as the algebraic sum of the rate of its production (or build-up) and the rate of its loss. That is

$$F\left(\frac{d\rho_m}{d\gamma}, \frac{d\rho_f}{d\gamma}, \dots\right) = g(\rho_m, \rho_f, \dots) - h(\rho_m, \rho_f, \dots) \quad 5.10$$

The first term at the right of equation (5.10) represents the rate of buildup of dislocation densities while the second term represents the rate of loss. In this model the evolution of dislocation densities is given by<sup>16,102</sup>:

$$\frac{d\rho_m}{d\gamma} = k_1\rho_m^{1/2} - k_2\rho_m\rho_f^{1/2} \quad 5.11a$$

$$\frac{d\rho_f}{d\gamma} = k_3\rho_f^{1/2} - k_4\rho_f \quad 5.11b$$

where  $k_1$ ,  $k_2$ ,  $k_3$  and  $k_4$  are rate constants. The first terms of equation (5.11) are derived from the work of Kocks et al<sup>103</sup>, who gave a general description of dislocation generation as:

$$\frac{d\rho_i}{dt} = \rho_s \frac{v}{Y_b} \quad 5.12$$

Where,  $i = m$  or  $f$ , indicates the dislocation species

$\rho_s$  = the density of dislocation source

$v$  = mean dislocation velocity and

$Y_b$  = average distance between emitted dislocations.

According to Orowan<sup>104</sup> plastic shear strain rate  $\dot{\gamma}_p$ , due to mobile dislocations of density  $\rho_m$  and Burgers vector  $b$ , moving with an average velocity  $v$ , is given by:

$$\frac{d\gamma_p}{dt} = \rho_m b v \quad 5.13$$

Substituting  $v = \frac{k_1}{b\rho_m}$ , in equation (5.13) gives

$$\dot{\rho}_m = \left( \frac{\rho_s}{Y_b} \right) \frac{k_1}{\rho_m b} \quad 5.14$$

Several possibilities exist for  $\rho_s$  and  $Y_b$ <sup>2,44,104</sup> depending on which species of dislocation production is considered. For  $i = m$ , it is considered that  $\rho_s$  is proportional to mobile dislocation density  $\rho_m$  and  $Y_b$  is proportional to the mean free path, i.e.,  $Y_b \propto \rho_m^{-1/2}$ . Thus, the rate of generation of mobile dislocation density according to equation (5.14) becomes:

$$\dot{\rho}_m \alpha \left( \frac{\rho_m}{\rho_m^{-1/2} \rho_m} b \right) = k_1 \rho_m^{1/2} \dot{\gamma} \quad 5.15$$

which implies that  $\frac{d\rho_m}{d\gamma} = k_1 \rho_m^{1/2}$ . For  $i = f$ , mobile dislocations are assumed to act as sources for the generation of forest dislocations, with the mean distance between them being inversely proportional to its density. That is,  $\rho_s = \rho_m$  and  $Y_b \propto \rho_f^{-1/2}$ . In this case, equation (5.14) becomes:-

$$\dot{\rho}_f \alpha \frac{\left( \frac{\rho_m}{\rho_f^{-1/2}} \right) k_1}{\rho_m b} = k_1 \rho_f^{1/2} \dot{\gamma} \quad 5.16$$

And which yields  $\frac{d\rho_m}{d\gamma} = k_3 \rho_f^{1/2}$

The second term of equation (5.11a) which represents the loss of mobile dislocation density is due to immobilization of mobile dislocation density and occurs by one or the other of two main processes: either as a result of interaction between mobile-mobile dislocations or, as a result of interaction between mobile-forest dislocations. These two processes are

considered to act cooperatively and so, differ from that of other schemes<sup>10,44,105</sup> where immobilization by these dislocation species is assumed to occur independently and in an additive manner. For any given strain rate the immobilization due to mobile - mobile dislocation interactions is proportional to the mobile dislocation density  $\rho_m$  while that due to mobile-forest dislocations is inversely proportional to the mean distance between obstacles which, in the case of forest dislocations, is proportional to  $\rho_f^{-1/2}$ . Hence, the overall rate of immobilization becomes  $k_2 \rho_m \rho_f^{1/2}$ . An increase in mobile dislocation density will enhance mobile-mobile interactions while an increase in forest dislocation density will reduce the inter-obstacle spacing (i.e. reduce the mean free path) and enhance interactions between mobile and forest dislocations depending on the initial state of the material. The dislocation species with higher density will dominate the immobilization process, with the other complementing them. In the case of equation (5.11b), the second term representing the rate of loss of forest dislocation density with strain may be due to dynamic recovery processes such as rearrangement of and or breakdown of dislocation cell substructures, cross-slip and annihilation of screw dislocations. All these processes, which are assumed to act co-operatively and complementary to each other, are proportional to the instantaneous forest dislocation density.  $\rho_f$ .

Equation (5.11) becomes zero either at peak conditions and or the saturation stage. It is important to note that peak point is not necessarily a saturation stage, as is the case in cyclic loading, where steady state cycling precedes the saturation stage, or steady-state creep. Also, in strain-amplitude cycling, where cyclic hardening/softening occurs, peak stresses again precede the saturation stage. It is only in the case of monotonic loading behaviour that the peak stress may reach the saturation point.

Let the mobile dislocation density at the peak point be  $\rho_{mp}$  then at this

stage equation (5.16a) becomes zero, that is

$$0 = k_1 \rho_{mp}^{1/2} \left[ 1 - \left( \frac{k_2}{k_1} \right) \rho_{mp}^{1/2} \rho_f^{1/2} \right] \quad 5.17$$

So that  $\frac{k_1}{k^2}$  in equation (5.11a) yields

$$\frac{d\rho_m}{d\gamma} = k_1 \rho_m^{1/2} \left[ 1 - \frac{(\rho_m^{1/2} \rho_f^{1/2})}{(\rho_{mp}^{1/2} \rho_f^{1/2})} \right] \quad 5.18$$

But at the peak condition all the mobile dislocations are fully blocked as far as the loading direction is concerned. They may be able, however, to move in the opposite direction during unloading or reverse loading. In this fully blocked condition, the peak mobile dislocations are equivalent to peak forest dislocations with dislocation density given as  $\rho_{mp} = R\rho_f$ , where  $R$  is a numerical constant less than unity. Substituting  $\rho_{mp} = R\rho_f$  in equation (5.18) we have:-

$$\begin{aligned} \frac{d\rho_m}{d\gamma} &= k_1 \rho_m^{1/2} \left[ 1 - \frac{(\rho_m^{1/2} \rho_f^{1/2})}{R \rho_f^{1/2} \rho_f^{1/2}} \right] \\ &= k_1 \rho_m^{1/2} \left[ 1 - \frac{\rho_m^{1/2}}{R \rho_f^{1/2}} \right] \end{aligned} \quad 5.19$$

$R$  may be a constant or may vary with peak stress, Assuming that  $R$  is a constant, then it may be determined at the steady stage when

$\rho_m = \rho_{ms} = \rho_f = \rho_{fs}$  and  $\frac{d\rho_m}{d\gamma} = 0$ . Thus,  $1/R = \left( \frac{\rho_{fs}}{\rho_{ms}} \right)^{1/2}$ . Equations

(5.11b) and (5.19) together completely describe the deformation behaviour in terms of the dislocation densities. The behaviour may also be expressed in terms of stress by substituting equations (5.19) and (5.11b) into equations (5.9) and (5.8), respectively, and combining them with equations (5.7) and (5.11b) as:

$$\frac{d\sigma_{sc}}{d\gamma} = \theta_{11} \left[ 1 - \frac{C_o \sigma_{sc}}{\tau_t} \right] \quad 5.20a$$

$$\frac{d\tau_f}{d\gamma} = \theta_0 \left[ 1 - \frac{\tau_f}{\tau_{fs}} \right] \quad 5.20b$$

where  $\theta_{11} = 0.5\alpha\mu b k_1$ , is the initial slope of the stress-strain curve,  $C_o = 1/R^{1/2}$ ,  $\theta_0 = 0.5\alpha\mu b k_3$  is the initial slope of the athermal flow stress-strain curve; and  $\tau_{fs} = \frac{k_3\alpha\mu b}{k_4}$  is the saturation value of the athermal flow

strength. Equation (5.20a) shows that the slope of the stress-strain curve depends not only on the applied stress but rather, on the ratio of applied stress-to-internal flow stress and, that, this slope vanishes whenever the ratio reaches a value of  $1/C_o$ . Also equation (5.20b) is similar to equation (5.7), due to Kocks<sup>14</sup> except that  $\tau_{fs}$  replaces  $\tau_{max}$  in the Kocks's equation, since saturation does not necessarily occur at the maximum forest (or obstacle) dislocation density,  $\rho_{f\ max}$  but can also occur at an obstacle dislocation density less than  $\rho_{f\ max}$ . It is only in the case of monotonic loading that  $\rho_f$  may reach  $\rho_{f\ max}$ . Thus, equation (5.21b) accommodates both monotonic and cyclic cases.

For a polycrystalline material,  $\theta_{11} = \mu$ , the temperature-compensated shear modulus of elasticity of the material, thus  $k k_1 = 2(\alpha b)^{-1} 1$ . Work on fcc metals<sup>10,14,103</sup> indicates that the initial hardening rate  $\theta_0$  for monotonic loading behaviour has a value between 0.02-0.06 $\mu$ . The value of  $C_o$  is also determined, from monotonic behaviour at saturation or steady state, as the ratio between the athermal flow strength at saturation  $\tau_{fs}$ , and saturation applied shear stress  $\sigma_{scs}$ . Hence we have  $C_o = \frac{\tau_{fs}}{\sigma_{scs}}$ . In terms of

time equations (5.20) becomes;-

$$\dot{\epsilon}_{sc} = \dot{\epsilon}_0 \left[ 1 - \frac{C_o \sigma_{sc}}{\tau_f} \right] \quad 5.21a$$

$$\dot{\epsilon}_f = \dot{\epsilon}_p \theta_o \left[ 1 - \frac{\tau_f}{\tau_{fs}} \right] \quad 5.21b$$

Using modified versions of the above equations with relevant programmes like Microsoft Excel, Matlab / SIMULINK programmes; plastic deformation and creep under monotonic loading conditions can be described. What follows below is the case for polycrystalline low alloy steel.

### 5.2.1 Calculation of Plastic Deformation

In many approaches, descriptions of plastic deformation are based on the Norton creep law in which the axial plastic strain rate  $\dot{\epsilon}$  can be written in terms of the applied stress  $\sigma$  as:

$$\dot{\epsilon} = \dot{\epsilon}_0 \left( \frac{\sigma}{\sigma_o} \right)^m \quad 5.22$$

Where  $m$  is a constant with the temperature dependence contained in  $\dot{\epsilon}_0$  and  $\sigma_o$  is the value of the stress to produce an arbitrarily chosen strain rate of  $\dot{\epsilon}_0$ . In many instances results are relatively insensitive to the value of  $\dot{\epsilon}_0$  in which case it may be taken to be constant representing elastic collapse of the structure.

More recently, this purely empirical relationship was modified so as to describe plasticity due to dislocation glide at lower temperatures and higher stresses and power law creep due to dislocation climb at lower stresses and higher temperatures. Results are interpreted depending on the deformation mechanism been considered.

In describing plasticity due to glide,  $\sigma_o$  is replaced by  $\hat{\sigma}$  which is interpreted as a variable representing the internal structural state of the material (known here as the “material state stress”) and the constant  $m$  taken to be temperature dependent with:-<sup>38</sup>

$$m = C/kT \quad 5.23$$

where  $C$  is a constant,  $T$ , the absolute temperature and  $k$  is Boltmann's constant. In recent developments<sup>5, 12</sup>,  $m$  is given by:-

$$m = V\sigma/kT \quad 5.24$$

Where  $V$  is the activation energy with  $\sigma$ ,  $k$  and  $T$  retaining their usual meanings.

For many applications involving power law creep, the Dorn equation is frequently used. Equation (5.22) has a form similar to the Dorn Equation for power law creep with  $m$  being constant.

$$\dot{\epsilon} = \frac{D}{kT} \left( \frac{\sigma}{\hat{\sigma}} \right)^{\frac{v\sigma}{kT}} \quad 5.25$$

$D$  is lattice diffusion and is temperature dependent. It can be represented as:-

$$D = D_0 \exp\left(-\frac{Q_f}{RT}\right) \quad 5.26$$

where  $R$  is the universal gas constant and  $Q_f$  is the activation energy for flow. In describing power law creep caused by dislocation climb using the Dorn equation, the stress is normalized with respect to the temperature dependent elastic modulus in some approaches.<sup>2</sup> Here, the temperature dependence is being contained in a term including the diffusion coefficient, since at high temperatures climb is generally lattice

diffusion controlled. The velocity,  $V_c$  at which an edge dislocation climbs under local normal stress acting parallel to its burgers vector, is:-

$$V_c = \frac{D_c \sigma_n \Omega}{bkT} \quad 5.27$$

Combining equation (5.27) and expressions  $\dot{\epsilon} = \rho_m bv$  and  $\rho_m = \alpha \left( \frac{\sigma_s}{Eb} \right)$

we obtain:

$$\dot{\epsilon} = \frac{ADE_b}{kT} \left( \frac{\sigma}{E} \right)^m \quad 5.28$$

Where  $\Omega$  is approximated by  $b^3$  and  $A$  is a dimensionless constant represented all constants.

Measurement of the activation energy in power law breakdown regime often gives values exceeding that of self diffusion. This is sometimes taken to indicate that the recovery process differs from that of climb controlled creep. Some of the difference, however, may simply reflect the temperature-dependence of the shear modulus, which has a greater effect when the stress-dependence is greater. An alternative relationship that reduces to the Dorn equation at lower stresses but is often better than equation (5.28) for describing transition region between plasticity and power law creep, which is known as power law breakdown is:-<sup>2</sup>

$$\dot{\epsilon} = \frac{A'DE_b}{kT} \left( \sinh \alpha \frac{\sigma}{E} \right)^m \quad 5.29$$

$A'$  and  $\alpha$  are constants with  $m$  having the same value as in equation (5.27). Only steady state creep at constant structure can be described in either case. Neither equations (5.27) and (5.28) can adequately describe the creep curve behavior. To analyze results equation (5.29) was re-written as<sup>105</sup>:-

$$\dot{\epsilon} = \frac{A'DE_b}{kT} \left( \sinh \alpha \frac{\sigma}{\sigma_0} \right)^n \exp\left(-\frac{Q_f}{RT}\right) \quad 5.30$$

The effects of structure evolution are of importance in this investigation so it has been assumed that this can be introduced into the power law creep equation by normalizing the applied stress ( $\sigma_a$ ) with respect to the material state stress ( $\sigma_0$ ). This differs from many other approaches in which the effect of an internal stress ( $\sigma_0$ ) is represented by a term subtracted from the applied stress in the power law creep equation<sup>7</sup> or like Miller<sup>82</sup> we have  $\left(\frac{\sigma_a - \sigma_0}{G}\right)$ . The advantage of this approach is that the creep rate could be brought closer together at the relevant temperature. The modulus of elasticity, as is stipulated above, is temperature dependent with a functional relationship between internal stress and the activation energy. In models utilizing the internal stress concept, it is generally recognized that the internal stress is unstable, varying with temperature, stress, time and the heterogeneity of the microstructure as has been noted<sup>71-74</sup>.

Normalizing stress with respect to material state stress in this study has a possible advantage in that both plasticity and power law creep have the same form of the Norton equation. Furthermore, it has been demonstrated by some researchers that normalizing stress with some material parameter provides better correlation of data. For example, Evans et al<sup>83</sup> observed that creep data for all materials superimpose when the effective stress is normalized by the proof or yield stress,

$\dot{\epsilon} = B'' \left( \frac{\sigma - \sigma_0}{\sigma_y} \right)^n$ ; a considerable improvement for the maximum to minimum ratio of  $\left( \frac{\sigma_a - \sigma_0}{G} \right)$  obtained by other approaches<sup>97</sup>.

Furthermore, when flow stresses at different temperatures and strain rates

are plotted in terms of  $kT \log\left(\frac{\dot{\epsilon}}{\epsilon_0}\right)$  against stress, should there be any changes in deformation mechanisms, these should be readily identifiable by discontinuities in the curve, prompting further analysis. With this approach it was possible to correlate tensile and creep data. Relevant parameters intrinsic to the material are determined and adjustment effected. The rationale was to use parameters obtained from the tensile data to determine creep properties of the low alloy steel. This would not have been possible had the approach been used that normalizes the stress to the modulus, which depends on temperature. This would have required making adjustment for changes in temperature in the model.

The two distinct types of behavior observed in section (5.1.1) may probably be linked to a change in a deformation mechanism occurring at a yield stress of about 550MPa. Values for the apparent activation volume,  $V$ , of  $8.90 \times 10^{-28} \text{ m}^3$  were obtained, together with a value for the material state stress,  $\hat{\sigma}$ , of 1052 MPa in figure (5.2) for values corresponding to yield stresses greater than 550MPa, which were analyzed in terms of glide deformation kinetics as expressed by equations (5.22) and (5.25).

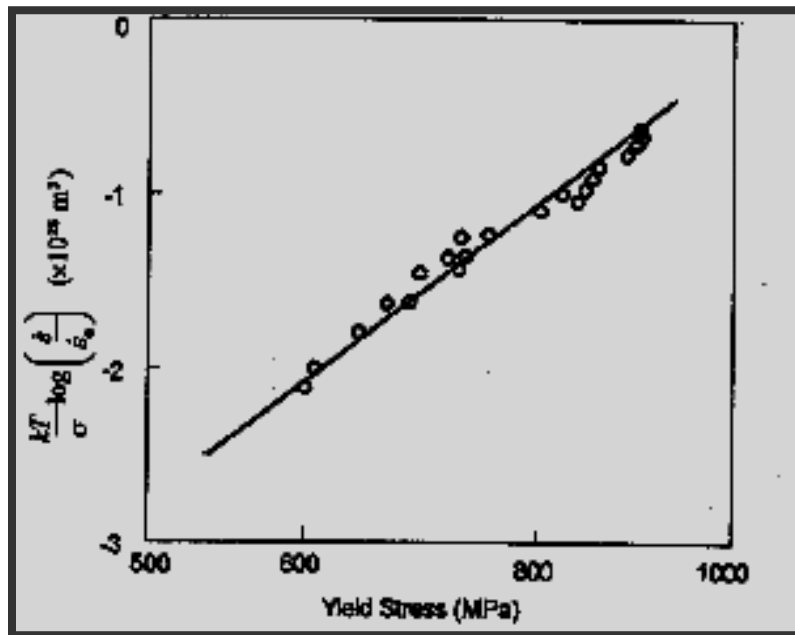


Figure 5.2: Strain rate plotted against tensile yield stress in terms of glide equation 5.27 and 5.30 from specimens tested at strain rates and temperatures having yield stress above 550MPa. Experimental results are shown as symbols and the solid curve represents the best-fit straight line

The results for yield stresses less than 550 MPa which were generally from tests at higher temperatures (above about 500°C) were analyzed using equation (5.22) and (5.30). To do this, a value of apparent activation energy was first found in a way that points on a log-log plot of

$kT \exp\left(\frac{Q_f}{RT}\right)$  versus  $\sigma$  lay on a straight line. Although such a value was

found in the region of 400 kJ mol<sup>-1</sup>, points did not lie on a straight line. They tended toward linearity at lower stresses but lay on a steeping curve at higher stresses in much the same way as these results appear in figure 5.1. It was surmised, therefore, that some of the results lay in the transition region between glide and climb processes referred to as power law breakdown<sup>2</sup>. An empirical relationship, equation (5.35) that has been used to describe power law breakdown, which reduces to power

law creep at lower stresses is used to plot results as  $kT \exp\left(\frac{Q_f}{RT}\right)$

versus  $\left(\sinh\left(a\frac{\sigma}{\hat{\sigma}}\right)\right)$ , a value for  $Q_f$  was found in a way that points lay on a single curve using log-log axes, and a value of  $a$  was found which linearised the curve

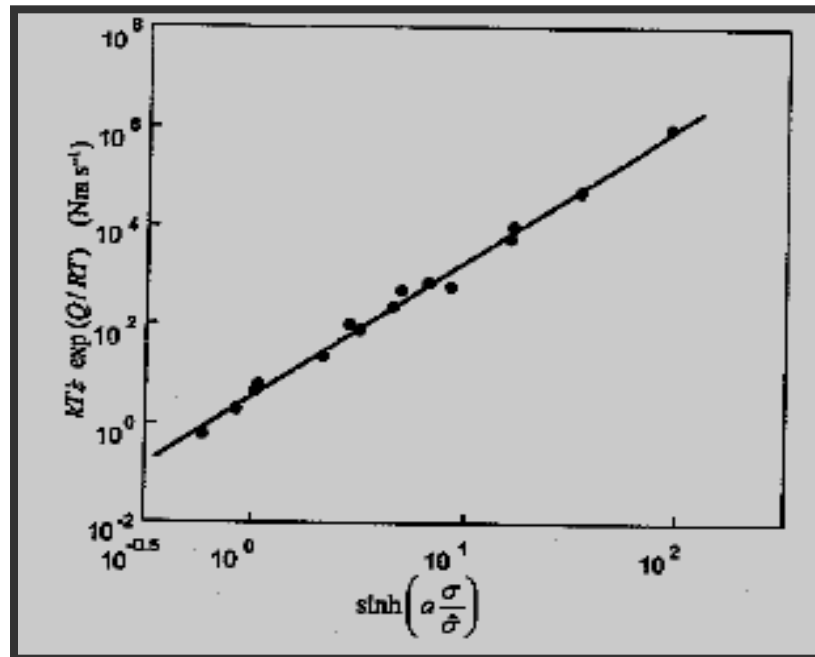


Figure 5.3: Strain rate plotted against tensile yield stress in terms of the power law breakdown, equation 5.6 from specimen tested at different strain rates and temperatures having yield stresses below 550MPa. Experimental results are shown as symbols and the solid curve represents the best-fit straight line.

As shown on figure (5.3), the results appear to fit equation (5.30) reasonably well with values of  $Q_f = 450 \text{ kJ mol}^{-1}$  and  $a = 10$ . The value of the apparent activation energy for creep is much higher than that for self-diffusion in iron. However, it is reasonably close to values of about  $380 \text{ kJ mol}^{-1}$  found for alloy steels<sup>49</sup>. The results in figure (5.3) are not highly sensitive to the value chosen for  $Q_f$  so that taking a lesser value still gives a fairly good fit to the results. From the slope and intercept of the curve,  $n$  was determined as 2.74 and  $A$  as  $3.63 \text{ Js}^{-1}$

In its simplistic form, equation (5.29) is incapable of explaining certain experimental facts, notably an increase in the exponent and a drop in the activation energy for creep at lower temperatures. To do so it is necessary to assume that the transport of matter via dislocation core diffusion contributes significantly to the overall diffusion transport of matter and under certain circumstances- becomes the dominant transport mechanism.

The use of only two parameters  $n$  and  $\alpha$  to describe three quantities is itself not satisfactory;  $n$  describes the power law,  $\alpha$  prescribes the stress level at which the power law breakdown occurs, and  $n$  and  $\alpha$  describe the strength of the exponential stress dependence. Lacking any physical model, it must be considered fortuitous that any set of  $n$  and  $\alpha$  can correctly describe the behavior over a wide range of stresses.

In analyzing the low stress results, the assumption has been made that the material state stress  $\hat{\sigma}$  determined from the glide form of the deformation equations is the same as that used in the power law breakdown formulation, equation (5.30). Thus a value of  $\hat{\sigma} = 1052$  MPa was used to determine material parameters in equation (5.30). In view of the somewhat empirical nature of the two deformation equations, the assumptions cannot be regarded as necessarily valid and need to be justified by later results. However, if as in the case of the present work, tests at room temperature are used to determine  $\hat{\sigma}$  value which is to be used for creep results obtained from conditions where the deformation mechanism is different, some sort of relationship between the two quantities is necessary. As is demonstrated below, a one to one correspondence seems to give satisfactory results for this material but it may not be the case for other types of alloy.

In spite of these reservations, this approach gave a good description of the result. Values of  $n$  are prescribed by the power law, and the adjustable parameter is  $\alpha$ .

## 5.2.2 Determination of Softening Kinetics

Softening processes in low alloy steels are expected to be due to recovery of dislocation of forest structures and /or precipitate growth. Previous work has suggested that the former controls softening during creep<sup>12</sup> and this is assumed to be the dominant effect in the present work over the test conditions investigated. The simplest kinetics equation describing dislocation recovery considers the annihilation of a pair of dislocations and can be written in terms of a simple second order process as<sup>45</sup>

$$\frac{d\rho}{dt} = -\beta^i \rho^2 \quad 5.31$$

with  $\rho$  representing the dislocation density. The rate constant  $B$  is expected to be temperature dependent through a term such as  $B^1 = B_0^1 / kT \exp\left(-\frac{Q_r}{RT}\right)$  where  $Q_r$  is the activation energy for recovery and  $B_0^1$  is a constant. From the relationship between stress and dislocation density  $\sigma = \alpha b \rho^{1/2}$  ( $b$  is the magnitude of the burgers vector and  $\alpha$  is a constant) and assuming that  $\rho$  refers to the forest dislocation density, which, in turn, reflects the value of the material state stress, equation (5.31) becomes.

$$\frac{d\hat{\sigma}}{dt} = -\frac{B}{kT} (\hat{\sigma} - \hat{\sigma}_o)^3 \quad 5.32$$

where  $b$  and  $\alpha$  are included in  $B$ . Here an additional assumption is made that there is a minimum value of  $\rho$  and hence a minimum value of the material state stress, denoted by  $\hat{\sigma}_o$ , which is attributed by recovery processes within the range of conditions investigated.

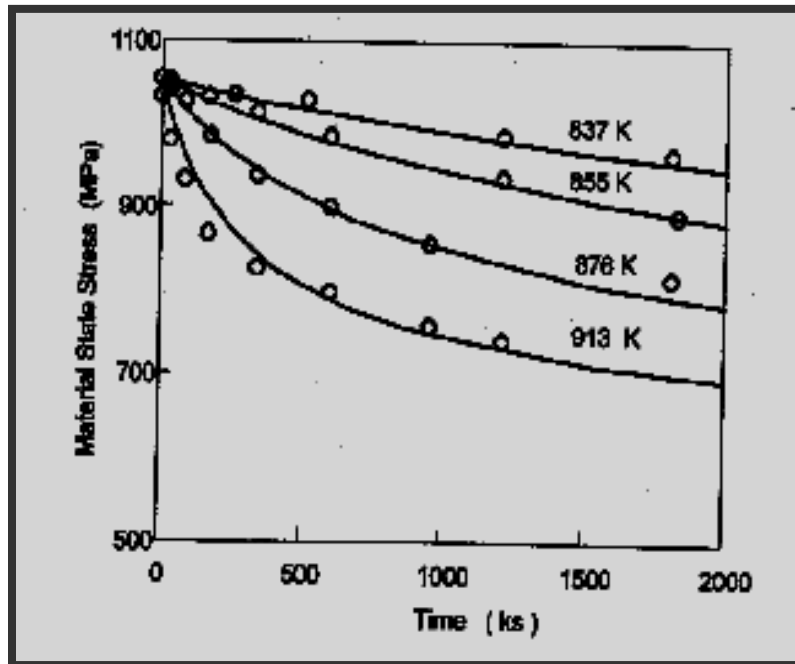


Figure 5.4: Values of the material state stress, determined using Equations (5.1) and (5.3) from specimens which had been aged in a Furnace for different times and temperatures. Solid curves were calculated using equation 5.8 and the material parameter values.

Recovery of the material state stress at yield plotted against time at four furnace holding temperatures is shown in figure (5.4). Since results were from tensile tests at room temperature, equations (5.22) and (5.25) were used to calculate values of  $\hat{\sigma}$ . Solid curves in figure 5.4 indicate values calculated from an integrated form of equation (5.32). The value of  $Q_r$  was assumed to be the same as the activation energy for self diffusion of iron, i.e.  $251 \text{ kJ mol}^{-1}$ .

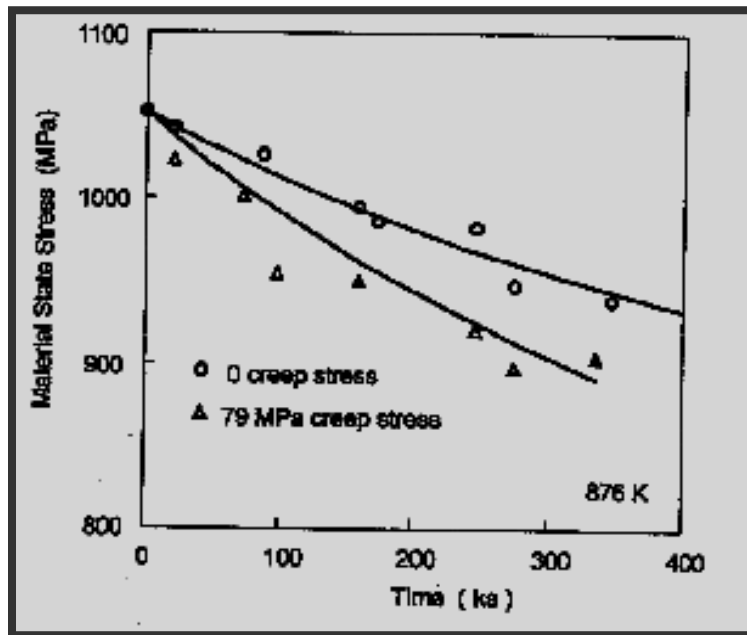


Figure 5.5: Softening curves of the material state stress against time for specimens aged in a furnace and from interrupted creep tests

A range of activation energies yielded reasonable results in figure (5.4) although not one as high as that found for deformation from figure (5.3). Values for  $\sigma_0$  of the same order of magnitude as that found for stress responsible for the mechanism change in figure (5.1) appeared to give good results. Thus the same value, i.e., 550 MPa was used. The value of the constant  $B$  in equation (5.32) was found to be  $1.5 \times 10^{-17} \text{ M}^5 \text{ N}^{-1} \text{ s}^{-1}$ .

As noted previously<sup>12</sup> alloy steels show enhanced softening when subjected to an applied load compared to static recovery at the same temperature. The material tested in this study also shows a similar effect, as illustrated in figure (5.5) for yield stress measurements obtained from interrupted creep specimens tested at 603°C with an initial axial stress of 79 MPa. These are true stress values making due allowance for creep deformation. Equations (5.31) and (5.32) imply that the driving force for recovery is the material state stress as reflected by the dislocation density. It may therefore be assumed that this driving force is increased by some function of the applied stress when the material is operating under creep conditions. The simplest function is to increase the material

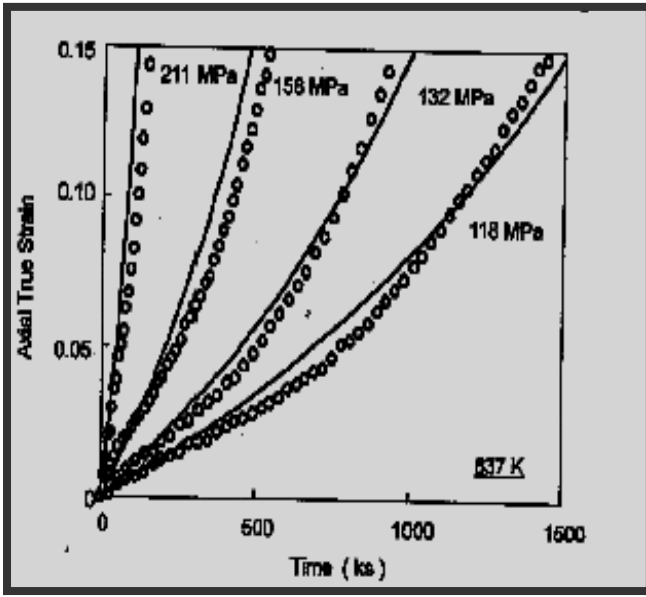
state stress by an amount equal to the applied stress. The lower solid curve in figure (5.5) shows the recovery calculated when the applied stress is added to  $\hat{\sigma}$  which, although showing reasonable agreement tends perhaps to underestimate the degree of softening. Assuming the effect to be additive, equation (5.32) could be modified to<sup>105</sup>:

$$\frac{d\hat{\sigma}}{dt} = -\frac{B}{kT} [(\hat{\sigma} + \sigma) - \sigma_0]^3 \quad 5.33$$

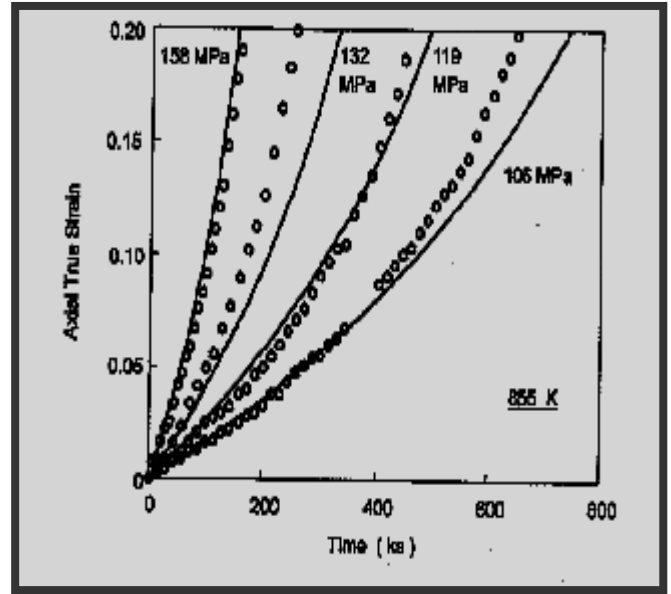
The condition may be expected to apply only to materials in which the principal mechanism of softening is recovery of a dislocation forest structure. In materials where softening is dominated by precipitate growth, it is to be expected that an expression describing accelerated growth should replace it.

### 5.2.3 Calculation of Creep Behavior

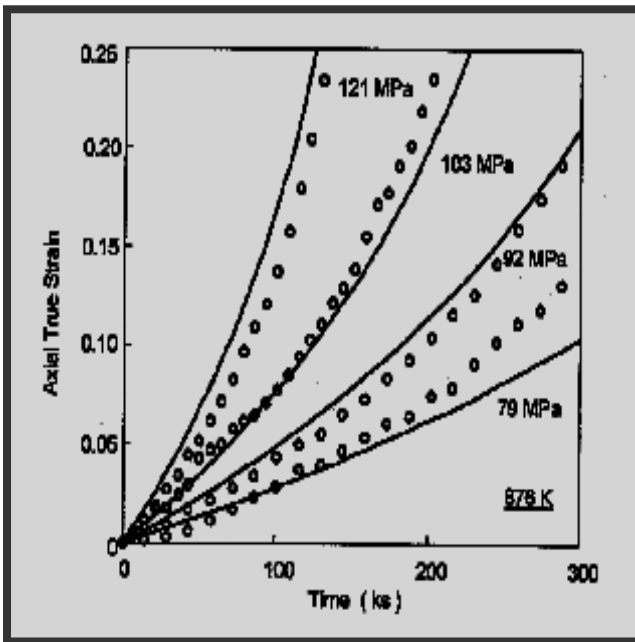
The creep results were carried out under conditions in which the maximum initial stress was 211MPa, i.e., under conditions where the deformation mechanism was in the power law/power law breakdown regime. Consequently equation (5.28) was used as the kinetic equation with equation (5.32) describing evolution. Material parameter values were as obtained from the tensile test programme with material parameters as listed above. Creep curves were calculated numerically using commercially available software. Figures (5.4 a-d) give the experimental and calculated results of creep curves obtained at different experimental temperatures.



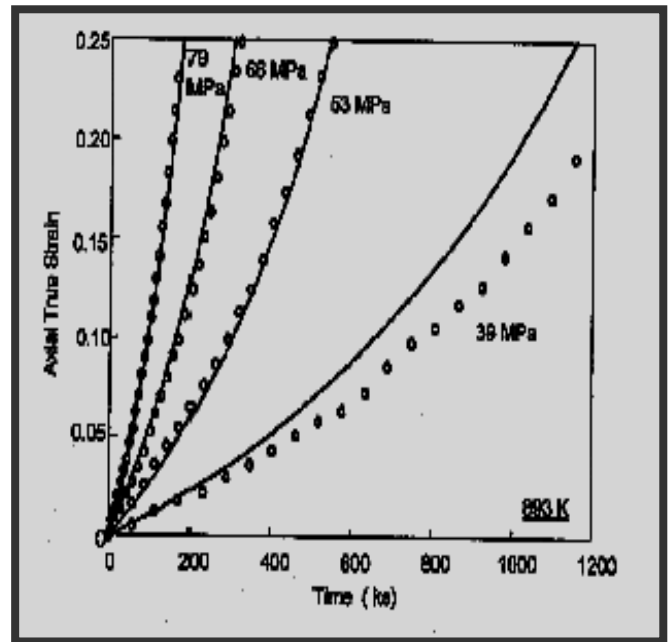
(a)



(b)



(c)



(d)

Figure 5.6: Experimental (symbols) and calculated (solid Curves) creep results for temperatures of (a)  $564^{\circ}\text{C}$ , (b)  $582^{\circ}\text{C}$  (c)  $603^{\circ}\text{C}$  and (d)  $620^{\circ}\text{C}$ . The stress values indicated are those at the start of each test.

Most studies concerned with high temperature creep have discussed the stress dependence of the secondary creep rate in terms of a power law

representation<sup>95</sup>. It was common to represent the  $\log\sigma/\log\dot{\epsilon}$  relationship by means of a straight line segment of gradient,  $n$ . With low alloy steel of the type used in this study, this approach would result in a decrease in  $n$  value. This decrease in  $n$  with increasing test duration has generally been interpreted in terms of changes in creep mechanism. Thus high  $n$  value dislocations are thought to be able to bow between or cut through the particles whereas, in the stress range when  $n$  is small, climb over particles or concentration of dislocation activity in the grain boundary regions is usually considered important. In contrast  $n$  values very close to unity are normally assumed to be associated with deformation taking place by stress-directed flow of vacancies without dislocation movement.

Micro-structural interaction occurring during plastic deformation is extremely complex and any models describing bulk phenomena such as creep curve and stress strain behavior are necessarily only approximations from empirical input. Many of the models proposed in the bulk of the literature differ considerably both in content and substance. In many approaches, the plastic behavior is conveniently modeled in terms of a pair of coupled differential equations, one of which describes the strain rate in terms of the externally imposed testing conditions and an internal structure variable and the other describing the evolution of the internal structure term.

### **5.3 INTERNAL STRESS MODELS RESULTS**

The concept of internal stress is very useful in the understanding of the creep behaviour of a wide range of precipitate hardened alloys, particularly so for the class of material used in this study<sup>3,82,73</sup>. It can be used to assess the influence of a change in microstructure due to long term ageing on the creep properties in micro structurally unstable alloys such as ferritic steels, in which, in some cases damage is thought to occur by micro-structural effect rather than by the usual cavity formation. The major obstacle with the concept is that extrapolation for long ageing time is

unreliable because of the unstable nature of these alloys. Models by Wilshire et al<sup>65-67</sup>,  $\dot{\epsilon} = A(\sigma - \sigma_0)^n \text{Exp}\left(-\frac{Q}{RT}\right)$ , D Miller<sup>82</sup>,  $\dot{\epsilon} = B\left(\frac{\sigma - \sigma_0}{G}\right)^n$  and Evans et al<sup>73</sup>,  $\dot{\epsilon} = B''\left(\frac{\sigma - \sigma_0}{\sigma_y}\right)^n$  highlighted in chapter two are further analyzed and comparison made with the present model adopted in this study. The above equations have been re-arranged for comparison with the modified Dorn's equation used in this study:-

*Wilshire et al*

$$\dot{\epsilon} = A \sigma_0^n \left(\frac{\sigma}{\sigma_0} - 1\right)^n \text{Exp}\left(-\frac{Q}{RT}\right) \quad 5.33$$

*D Miller*

$$\dot{\epsilon} = B \left(\frac{\sigma_0}{G}\right)^n \left[\frac{\sigma}{\sigma_0} - 1\right]^n \quad 5.34$$

*Evans et al*

$$\dot{\epsilon} = B'' \left(\frac{\sigma_0}{\sigma_y}\right)^n \left[\frac{\sigma}{\sigma_0} - 1\right]^n \quad 5.35$$

Equation (5.34) and (5.35) compare favourably with (5.22). The value of  $n$  in each case is estimated as 3.5. The creep rate and recovery have similar stress dependence with the stress and temperature dependence similar to that predicted by recovery theory. The value of  $n = 2.72$  quoted for the model used in this study differs from that quoted for the above models. Thus stress dependence is less in the present study. Because of the complex and unstable nature of  $\sigma_0$ , the use of tensile data obtained in this study to determine  $\sigma_0$  will introduce many ambiguities. Firstly,

approximating  $\sigma_0^n$ ,  $\left(\frac{\sigma_0}{G}\right)^n$  and  $\left(\frac{\sigma_0}{\sigma_y}\right)^n$  to some constant value is nearly

impossible since the change of  $\sigma_0$  with either  $G$  or  $\sigma_y$  is not clear cut because  $\sigma_0$  is controlled by a host of variables<sup>92</sup>. it's value depends on the applied stress, temperature and the heterogeneity of the material at

any given instance. Furthermore, because it is raised to some power any slight increase in the friction stress would be significant.

The data from the present study could be used in the internal stress technique if either measurement for the  $\sigma_0$  could be obtained or  $\sigma_0$  is approximated to  $\sigma_0^1$ . Definitive relationship between internal stress and the applied stress does not always emerge, possibly because the behavior patterns displayed may vary depending on the material examined and on the precise stress-temperature conditions selected for investigation. The temperature and stress range used here generally conform to those used by many authors for this class of material. For this class of alloys, the ratio  $\frac{\sigma_i}{\sigma}$  may be constant or may increase with decreasing stress when tested at low stresses and or,  $\sigma_i$  may appear to be independent of stress when measurements are made at high stresses. Thus it would be safe to say that tensile data obtained at high stresses in this study would be expected to have little or no influence on the internal stress. Furthermore, because of the short duration of test time, it would be safe to assume that significant micro structural changes did not take place to justify such measurement which in most cases is very difficult to perform particularly at low strain rate. Thus it would be safe to assume that changes in internal stress values as a result of micro-structural changes will have been very slight at high stresses, especially during the secondary creep rate when the internal stress would be expected to be nearly equal to the applied stress. Thus equation (5.40) could be approximated to reflect equation (5.27) and  $\sigma_0$  could be expected to serve the same function as  $\sigma_0^1$  in such instances. Little should be read into the relative magnitude of  $\sigma_0$  since, in any material, it is dependent on temperature. Furthermore, for this class of material, it is the tertiary creep that is extensive. Thus the above assumptions have the potential of rendering the approach of only limited use. In this study measurement of

$\sigma_0$  was not carried out and because of the reasons highlighted above, data from present work has not been used for comparative analysis.